

Quantum effects in the optical response of extended plasmonic gaps: validation of the quantum corrected model in core-shell nanomatryushkas

Mario Zapata,^{1,2,3} Ángela S. Camacho Beltrán,¹ Andrei G. Borisov,^{2,3,4} and Javier Aizpurua^{3,*}

¹Universidad de los Andes, Bogotá D.C., Colombia

²Institut des Sciences Moléculaires d'Orsay, UMR 8214 CNRS-Université Paris-Sud, Bâtiment 351, 91405 Orsay Cedex, France

³Materials Physics Center CSIC-UPV/EHU and Donostia International Physics Center DIPC, Paseo Manuel de Lardizabal 4, 20018 Donostia-San Sebastián, Spain

⁴andrei.borissov@u-psud.fr

*aizpurua@ehu.es

Abstract: Electron tunneling through narrow gaps between metal nanoparticles can strongly affect the plasmonic response of the hybrid nanostructure. Although quantum mechanical in nature, this effect can be properly taken into account within a classical framework of Maxwell equations using the so-called Quantum Corrected Model (QCM). We extend previous studies on spherical cluster and cylindrical nanowire dimers where the tunneling current occurs in the extremely localized gap regions, and perform quantum mechanical time dependent density functional theory (TDDFT) calculations of the plasmonic response of cylindrical core-shell nanoparticles (nanomatryushkas). In this axially symmetric situation, the tunneling region extends over the entire gap between the metal core and the metallic shell. For core-shell separations below 0.5 nm, the standard classical calculations fail to describe the plasmonic response of the cylindrical nanomatryushka, while the QCM can reproduce the quantum results. Using the QCM we also retrieve the quantum results for the absorption cross section of the spherical nanomatryushka calculated by V. Kulkarni *et al.* [Nano Lett. **13**, 5873 (2013)]. The comparison between the model and the full quantum calculations establishes the applicability of the QCM for a wider range of geometries that hold tunneling gaps.

© 2015 Optical Society of America

OCIS codes: (240.6680) Surface plasmons; (250.5403) Plasmonics.

References and links

1. M. E. Stewart, C. R. Anderton, L. B. Thompson, J. Maria, Stephen K. Gray, J. A. Rogers, and R. G. Nuzzo, "Nanostructured plasmonic sensors," *Chem. Rev.* **108**, 494–521 (2008).
2. S. S. Aćimović, M. P. Kreuzer, M. U. González, and R. Quidant, "Plasmon near-field coupling in metal dimers as a step toward single-molecule sensing," *ACS Nano* **3**, 1231–1237 (2009).
3. B. K. Juluri, N. Chaturvedi, Q. Z. Hao, M. Q. Lu, D. Velegol, L. Jensen, and T. J. Huang, "Scalable manufacturing of plasmonic nanodisk dimers and cusp nanostructures using salting-out quenching method and colloidal lithography," *ACS Nano* **5**, 5838–5847 (2011).

4. R. Ariely, A. Ofarim, G. Noy, and Y. Selzer, "Accurate determination of plasmonic fields in molecular junctions by current rectification at optical frequencies," *Nano Lett.* **11**, 2968–2972 (2011).
5. J. Kern, S. Großmann, N. V. Tarakina, T. Häckel, M. Emmerling, M. Kamp, J.-S. Huang, P. Biagioni, J. C. Prangma, and B. Hecht, "Atomic-scale confinement of resonant optical fields," *Nano Lett.* **12**, 5504–5509 (2012).
6. H. Duan, A. I. Fernández-Domínguez, M. Bosman, S. A. Maier, and J. K. W. Yang, "Nanoplasmonics: classical down to the nanometer scale," *Nano Lett.* **12**, 1683–1689 (2012).
7. R. W. Taylor, T.-Ch. Lee, O. A. Scherman, R. Esteban, J. Aizpurua, F. M. Huang, J. J. Baumberg, and S. Mahajan, "Precise subnanometer plasmonic junctions for SERS within gold nanoparticle assemblies using cucurbit[n]uril "glue",
ACS Nano **5**, 3878–3887 (2011).
8. M. Danckwerts, and L. Novotny, "Optical frequency mixing at coupled gold nanoparticles," *Phys. Rev. Lett.* **98**, 026104 (2007).
9. K. J. Savage, M. M. Hawkeye, R. Esteban, A. G. Borisov, J. Aizpurua, and J. J. Baumberg, "Revealing the quantum regime in tunnelling plasmonics," *Nature* **491**, 574–577 (2012).
10. J. A. Scholl, A. García-Etxarri, A. L. Koh, and J. A. Dionne, "Observation of quantum tunneling between two plasmonic nanoparticles," *Nano Lett.* **13**, 564–569 (2013).
11. D. R. Ward, F. Hueser, F. Pauly, J. C. Cuevas, and D. Natelson, "Optical rectification and field enhancement in a plasmonic nanogap," *Nat. Nanotechnol.* **5**, 732–736 (2010).
12. Y. Jin, C. Jia, S.-W. Huang, M. O'Donnell, and X. Gao, "Multifunctional nanoparticles as coupled contrast agents," *Nat. Commun.* **1**, 41, (2010).
13. D.-K. Lim, K.-S. Jeon, J.-H. Hwang, H. Kim, S. Kwon, Y. D. Suh, and J.-M. Nam, "Highly uniform and reproducible surface-enhanced Raman scattering from DNA-tailorable nanoparticles with 1-nm interior gap," *Nat. Nanotechnol.* **6**, 452–460 (2011).
14. L. Kelly, E. Coronado, L. L. Zhao, and G. C. Schatz, "The optical properties of metal nanoparticles: the influence of size, shape and dielectric environment," *J. Phys. Chem. B* **107**, 668–677 (2003).
15. R. Alvarez-Puebla, L. M. Liz-Marzán, and F. J. García de Abajo, "Light concentration at the nanometer scale," *J. Phys. Chem. Lett.* **1**, 2428–2434 (2010).
16. J. A. Schuller, E. S. Barnard, W. Cai, Y. C. Jun, J. S. White, and M. L. Brongersma, "Plasmonics for extreme light concentration and manipulation," *Nat. Mater.* **9**, 193–204 (2010).
17. N. J. Halas, S. Lal, W.-S. Chang, S. Link, and P. Nordlander, "Plasmons in strongly coupled metallic nanostructures," *Chem. Rev.* **111**, 3913–3961 (2011).
18. A. J. Pasquale, B. M. Reinhard, and L. D. Negro, "Engineering photonic-plasmonic coupling in metal nanoparticle necklaces," *ACS Nano* **5**, 6578–6585 (2011).
19. M. Quinten, A. Leitner, J. R. Krenn, and F. R. Aussenegg, "Electromagnetic energy transport via linear chains of silver nanoparticles," *Opt. Lett.* **23**, 1331–1333 (1998).
20. S. A. Maier, P. G. Kik, H. A. Atwater, S. Meltzer, E. Harel, B. E. Koel, and A. A. G. Requicha, "Local detection of electromagnetic energy transport below the diffraction limit in metal nanoparticle plasmon waveguides," *Nat. Mater.* **2**, 229–232 (2003).
21. E. Hao and G. C. Schatz, "Electromagnetic fields around silver nanoparticles and dimers," *J. Chem. Phys.* **120**, 357–366 (2004).
22. I. Romero, J. Aizpurua, G. W. Bryant, F. J. García de Abajo, "Plasmons in nearly touching metallic nanoparticles: singular response in the limit of touching dimers," *Opt. Express* **14**, 9988–9999 (2006).
23. P. K. Jain and M. A. El-Sayed, "Plasmonic coupling in noble metal nanostructures," *Chem. Phys. Lett.* **487**, 153–164 (2010).
24. H. Xu, E. Bjeneld, M. Käll, L. Börjesson, "Spectroscopy of single hemoglobin molecules by surface enhanced Raman scattering," *Phys. Rev. Lett.* **83**, 4357–4360 (1999).
25. C. E. Talley, J. B. Jackson, C. Oubre, N. K. Grady, C. W. Hollars, S. M. Lane, T. R. Huser, P. Nordlander, and N. J. Halas, "Surface-enhanced Raman scattering from individual Au nanoparticles and nanoparticle dimer substrates," *Nano Lett.* **5**, 1569–1574 (2005).
26. J. Theiss, P. Pavaskar, P. M. Echternach, R. E. Muller, and S. B. Cronin, "Plasmonic nanoparticle arrays with nanometer separation for high-performance SERS substrates," *Nano Lett.* **10**, 2749–2754 (2010).
27. B. Fazio, C. D'Andrea, F. Bonaccorso, A. Irrera, G. Calogero, C. Vasi, P. G. Gucciardi, M. Allegrini, A. Toma, D. Chiappe, C. Martella, and F. B. de Mongeot, "Re-radiation enhancement in polarized surface-enhanced resonant Raman scattering of randomly oriented molecules on self-organized gold nanowires," *ACS Nano* **5**, 5945–5956 (2011).
28. L. Gunnarsson, T. Rindzevicius, J. Prikulis, B. Kasemo, M. Käll, S. Zou, and G. C. Schatz, "Confined plasmons in nanofabricated single silver particle pairs: experimental observations of strong interparticle interactions," *J. Phys. Chem. B* **109**, 1079–1087 (2005).
29. P. K. Jain, W. Huang, and M. A. El-Sayed, "On the universal scaling behavior of the distance decay of plasmon coupling in metal nanoparticle pairs: a plasmon ruler equation," *Nano Lett.* **7**, 2080–2088 (2007).
30. R. T. Hill, J. J. Mock, A. Hucknall, S. D. Wolter, N. M. Jokerst, D. R. Smith, and A. Chilkoti, "Plasmon ruler with Ångström length resolution," *ACS Nano* **6**, 9237–9246 (2012).

31. X. Ben and H. S. Park, "Size-dependent validity bounds on the universal plasmon ruler for metal nanostructure dimers," *J. Phys. Chem. C* **116**, 18944–18951 (2012).
32. N. Liu, M. Hentschel, T. Weiss, A. P. Alivisatos, and H. Giessen, "Three-dimensional plasmon rulers," *Science* **332**, 1407–1410 (2011).
33. A. Stolz, J. Berthelot, M-M Mennemanteuil, G. Colas des Francs, L. Markey, V. Meunier, and A. Bouhelier, "Nonlinear photon-assisted tunneling transport in optical gap antennas," *Nano Lett.* **14**, 2330–2338, (2014).
34. J. Berthelot, G. Bachelier, M. Song, P. Rai, G. Colas des Francs, A. Dereux, and A. Bouhelier, "Silencing and enhancement of second-harmonic generation in optical gap antennas," *Opt. Express* **20**, 10498–10508 (2012).
35. T. Hanke, G. Krauss, D. Trüttelein, B. Wild, R. Bratschitsch, and A. Leitenstorfer, "Efficient nonlinear light emission of single gold optical antennas driven by few-cycle near-infrared pulses," *Phys. Rev. Lett.* **103**, 257404 (2009).
36. S. Paloma, M. Danckwerts, and L. Novotny, *J. Opt. A: Pure Appl. Opt.* **11**, 114030 (2009).
37. W. Cai, A. P. Vasudev, and M. L. Brongersma, "Electrically controlled nonlinear generation of light with plasmonics," *Science* **333**, 1720–1723 (2011).
38. A. Bouhelier, M. Beversluis, A. Hartschuh, and L. Novotny, "Near-field second-harmonic generation induced by local field enhancement," *Phys. Rev. Lett.* **90**, 013903 (2003).
39. M. Kauranen and A. V. Zayats, "Nonlinear plasmonics," *Nature Photon.* **6**, 737–748 (2012).
40. S. F. Tan, L. Wu, J.K.W. Yang, P. Bai, M. Bosman, and C. A. Nijhuis, "Quantum plasmon resonances controlled by molecular tunnel junctions," *Science* **343**, 1496–1499 (2014).
41. G. Hajisalem, M. S. Nezami, and R. Gordon, "Probing the quantum tunneling limit of plasmonic enhancement by third harmonic generation," *Nano Lett.* **14**, 6651–6654 (2014).
42. W. Zhu and K. B. Crozier "Quantum mechanical limit to plasmonic enhancement as observed by surface-enhanced Raman scattering," *Nature Commun.* **5**, 4228 (2014).
43. J. Zuloaga, E. Prodan, and P. Nordlander, "Quantum description of the plasmon resonances of a nanoparticle dimer," *Nano Lett.* **9**, 887–891 (2009).
44. D. C. Marinica, A. K. Kazansky, P. Nordlander, J. Aizpurua, and A. G. Borisov, "Quantum plasmonics: nonlinear effects in the field enhancement of a plasmonic nanoparticle dimer," *Nano Lett.* **12**, 1333–1339 (2012).
45. R. Esteban, A. G. Borisov, P. Nordlander, and J. Aizpurua, "Bridging quantum and classical plasmonics with a quantum-corrected model," *Nature Commun.* **3**, 825 (2012).
46. J. Zuloaga, E. Prodan, and P. Nordlander, "Quantum plasmonics: optical properties and tunability of metallic nanorods," *ACS Nano* **4**, 5269–5276 (2010).
47. L. Stella, P. Zhang, F. J. García-Vidal, A. Rubio, and P. García-González, "Performance of nonlocal optics when applied to plasmonic nanostructures," *J. Phys. Chem. C* **117**, 8941–8949 (2013).
48. T. V. Teperik, P. Nordlander, J. Aizpurua, and A.G. Borisov, "Robust subnanometric plasmon ruler by rescaling of the nonlocal optical response," *Phys. Rev. Lett.* **110**, 263901 (2013).
49. T. V. Teperik, P. Nordlander, J. Aizpurua, and A. G. Borisov, "Quantum effects and nonlocality in strongly coupled plasmonic nanowire dimers," *Opt. Express* **21**, 27306–27325 (2013).
50. K. Andersen, K. L. Jensen, N. A. Mortensen, and K. S. Thygesen, "Visualizing hybridized quantum plasmons in coupled nanowires: From classical to tunneling regime," *Phys. Rev. B* **87**, 235433 (2013).
51. R. Esteban, A. Aguirregabiria, A. G. Borisov, Y. M. Wang, P. Nordlander, G. W. Bryant, and J. Aizpurua, "The morphology of narrow gaps modifies the plasmonic response," *ACS Photonics* **2**, 295–305 (2015).
52. T. Atay, J.-H. Song, and A. V. Nurmikko, "Strongly interacting plasmon nanoparticle pairs: from dipole-dipole interaction to conductively coupled regime," *Nano Lett.* **4**, 1627–1631 (2004).
53. S. Marhaba, G. Bachelier, Ch. Bonnet, M. Broyer, E. Cottancin, N. Grillet, J. Lerme, J.-L. Vialle, and M. Pellarin, "Surface plasmon resonance of single gold nanodimers near the conductive contact limit," *J. Phys. Chem. C* **113**, 4349–4356 (2009).
54. M. Schnell, A. Garcia-Etxarri, A. J. Huber, K. Crozier, J. Aizpurua, and R. Hillenbrand, "Controlling the near-field oscillations of loaded plasmonic nanoantennas," *Nature Photon.* **3**, 287–291 (2009).
55. O. Pérez-González, N. Zabala, A. G. Borisov, N. J. Halas, P. Nordlander, and J. Aizpurua, "Optical spectroscopy of conductive junctions in plasmonic cavities," *Nano Lett.* **10**, 3090–3095 (2010).
56. O. Pérez-González, N. Zabala, and J. Aizpurua, "Optical characterization of charge transfer and bonding dimer plasmons in linked interparticle gaps," *New J. Phys.* **13**, 083013 (2011).
57. M. Hentschel, D. Dregely, R. Vogelgesang, H. Giessen, and N. Liu, "Plasmonic oligomers: the role of individual particles in collective behavior," *ACS Nano* **5**, 2042–2050 (2011).
58. C. David and F. J. García de Abajo, "Spatial nonlocality in the optical response of metal nanoparticles," *J. Phys. Chem. C* **115**, 19470–19475 (2011).
59. A. I. Fernández-Domínguez, A. Wiener, F. J. García-Vidal, S. A. Maier, and J. B. Pendry, "Transformation-optics description of nonlocal effects in plasmonic nanostructures," *Phys. Rev. Lett.* **108**, 106802 (2012).
60. G. Toscano, S. Raza, A.-P. Jauho, N. A. Mortensen, and M. Wubs, "Modified field enhancement and extinction by plasmonic nanowire dimers due to nonlocal response," *Opt. Express* **20**, 4176–4188 (2012).
61. G. Toscano, S. Raza, S. Xiao, M. Wubs, A.-P. Jauho, S. I. Bozhevolnyi, and N. A. Mortensen, "Surface-enhanced Raman spectroscopy (SERS): nonlocal limitations," *Opt. Lett.* **37**, 2538–2540 (2012).

62. Y. Luo, A. I. Fernandez-Dominguez, A. Wiener, S. A. Maier, and J. B. Pendry, "Surface plasmons and nonlocality: a simple model," *Phys. Rev. Lett.* **111**, 093901 (2013).
63. G. Toscano, C. Rockstuhl, F. Evers, H. Xu, N. A. Mortensen, and M. Wubs, "Self-consistent hydrodynamic approach to nanoplasmonics: resonance shifts and spill-out effects," arXiv:1408.5862 [physics.optics].
64. P. Zhang, J. Feist, A. Rubio, P. García-González, and F. J. García-Vidal, "Ab initio nanoplasmonics: The impact of atomic structure," *Phys. Rev. B* **90**, 161407(R) (2014).
65. J. D. Jackson, *Classical Electrodynamics*, 3rd ed. (Wiley, 1999).
66. R. Esteban, A. Zugarraurdi, P. Zhang, P. Nordlander, F. J. García-Vidal, A. G. Borisov, and J. Aizpurua, "A classical treatment of optical tunneling in plasmonic gaps: extending the quantum corrected model to practical situations," *Faraday Discuss.*, (2015), DOI: 10.1039/c4fd00196f.
67. S. Gao, P. Li, and F. Li, "Geometrical parameters controlled focusing and enhancing near field in infinite circular metal-dielectric multilayered cylinder," *Appl. Phys. Lett.* **102**, 123107 (2013).
68. Y. Hu, R. C. Flemming, R. A. Drezek, "Optical properties of gold-silica-gold multilayer nanoshells," *Opt. Express* **16**, 19579–19591 (2008).
69. R. Bardhan, S. Mukherjee, N. A. Mirin, S. D. Levit, P. Nordlander, and N. J. Halas, "Nanosphere-in-a-nanoshell: a simple nanomatryushka," *J. Phys. Chem. C* **114**, 7378–7383 (2010).
70. J. Qian, W. Wang, Y. Li, J. Xu, and Q. Sun, "Optical extinction properties of perforated gold-silica-gold multilayer nanoshells," *J. Phys. Chem. C* **116**, 10349–10355 (2012).
71. O. Peña-Rodríguez, A. Rivera, M. Campoy-Quiles, and U. Pal, "Tunable Fano resonance in symmetric multilayered gold nanoshells," *Nanoscale* **5**, 209–216 (2013).
72. C. W. Hsu, B. G. DeLacy, S. G. Johnson, J. D. Joannopoulos, and M. Soljačić, "Theoretical criteria for scattering dark states in nanostructured particles," *Nano Lett.* **14**, 2783–2788 (2014).
73. C. Ayala-Orozco, J. G. Liu, M. W. Knight, Y. Wang, J. K. Day, P. Nordlander, and N. J. Halas, "Fluorescence enhancement of molecules inside a gold nanomatryushka," *Nano Lett.* **14**, 2926–2933 (2014).
74. E. Román-Velázquez, and C. Nogues, "Designing the plasmonic response of shell nanoparticles: Spectral representation," *J. Chem. Phys.* **134**, 044116 (2011).
75. H. Xu, "Multilayered metal core-shell nanostructures for inducing a large and tunable optical field," *Phys. Rev. B* **72**, 073405 (2005).
76. V. Kulkarni, E. Prodan, and P. Nordlander, "Quantum Plasmonics: optical properties of a nanomatryushka," *Nano Lett.* **13**, 5873–5879 (2013).
77. C. Yannouleas, E. Vigezzi, and R. A. Broglia, "Evolution of the optical properties of alkali-metal microclusters towards the bulk: the matrix random-phase-approximation description," *Phys. Rev. B* **47**, 9849–9861 (1993).
78. Th. Fennel, K.-H. Meiwes-Broer, J. Tiggesbäumker, P.-G. Reinhard, P. M. Dinh, and E. Suraud, "Laser-driven nonlinear cluster dynamics," *Rev. Mod. Phys.* **82**, 1793–1842 (2010).
79. E. Prodan, P. Nordlander, and N. J. Halas, "Electronic structure and optical properties of gold nanoshells," *Nano Lett.* **3**, 1411–1415 (2003).
80. E. Prodan, P. Nordlander, and N. J. Halas, "Effects of dielectric screening on the optical properties of metallic nanoshells," *Chem. Phys. Lett.* **368**, 94–101 (2003).
81. J. M. Pitarke, V. M. Silkin, E. V. Chulkov, and P. M. Echenique, "Theory of surface plasmons and surface-plasmon polaritons," *Rep. Prog. Phys.* **70**, 1–87 (2007).
82. A. Liebsch, "Surface-plasmon dispersion and size dependence of Mie resonance: silver versus simple metals," *Phys. Rev. B* **48**, 11317–11328 (1993).
83. M. A. L. Marques, and E. K. U. Gross, "Time-dependent density functional theory," *Annu. Rev. Phys. Chem.* **55**, 427–455 (2004).
84. O. Gunnarsson and B. I. Lundqvist, "Exchange and correlation in atoms, molecules, and solids by the spin-density-functional formalism," *Phys. Rev. B* **13**, 4274–4298 (1976).
85. Cottancin, E.; Celep, G.; Lermé, J.; Pellarin, M.; Huntzinger, J. R. Vialle, and J. L. Broyer, "Optical properties of noble metal clusters as function of the size: comparison between experiments and semi-quantal theory," *Theor. Chem. Acc* **2006**, 116, 514–523.
86. H. Hövel, S. Fritz, A. Hilger, U. Kreibig, and M. Vollmer, "Width of cluster plasmon resonances: bulk dielectric functions and chemical interface damping," *Phys. Rev. B* **48**, 18178–18188 (1993).
87. P. Apell and D. R. Penn, "Optical properties of small metal spheres: surface effects," *Phys. Rev. Lett.* **50**, 1316–1319 (1983).
88. P. Apell, Å. Ljungbert, "Red shift of surface plasmons in small metal particles," *Solid State Commun.* **44**, 1367–1369 (1982).
89. H. Haberland, "Looking from both sides," *Nature* **494**, E1–E2 (2013).

1. Introduction

Modern technology allows for fabrication of metallic nanoparticles and nanoparticle assemblies of different geometry, structure, and composition [1–13]. This, in turn, opens a possibility to

engineer the plasmonic modes of these artificial nanostructures and thus the way they interact with light [14–20]. In this context much of the interest has been devoted to the nanostructures that form narrow plasmonic gaps between their constituent metallic surfaces [17]. The strong interaction of the plasmon-induced charge density across the gap results in the manyfold enhancement of the confined fields and in the hybridization of the plasmonic modes of the individual nanoparticles [21–23]. The field enhancement and the geometrical tunability provided by plasmon resonances find many practical applications including sensing [1, 24–27], plasmon rulers [2, 17, 28–32], and non linear optics [8, 11, 33–39], among others.

So far, the classical electrodynamics framework based on the local description of the metal dielectric function appeared adequate to describe optical properties of strongly coupled plasmonic nanoparticles separated by narrow gaps. However, recent experimental [4, 9–11, 40–42] and theoretical [9, 43–51] studies have demonstrated the importance of quantum mechanical effects when particle-to-particle separations are reduced below the nanometer. In this case, the non-local screening and the electron tunneling across the gap can reduce (and even quench) the field enhancement, and alter the optical response of the system. Because of the tunneling, a conductive contact between the nanoparticles can be established, prior to the direct geometrical overlap. As a consequence, the extinction resonances arising from the hybridization of the plasmonic modes of the individual nanoparticles disappear from the spectrum. At the same time, a set of charge transfer plasmon modes emerge as a consequence of the electron flow between the nanoparticles [52–57]. The use of nonlocal dielectric functions [15, 47, 58–61] captures part of the quantum behavior of such systems introducing a smooth variation of the screening electron density at the metal surface rather than one infinitely sharp, as assumed in the classical local approach. This solves the problem of the divergence of the electric fields and energy shifts of the plasmon resonances with decreasing junction width, as obtained in local classical theories [62]. The latest developments of the non-local hydrodynamic descriptions allow to introduce the realistic electron density profile at the surface so that full quantum results can be retrieved for individual nanoparticles [63] albeit at the price of growing the numerical complexity. However, to account for tunneling across narrow interparticle junctions requires a special treatment that goes beyond classical local or non-local hydrodynamic approaches.

Quantum tunneling thus imposes a real challenge to any theoretical description. Indeed, the simplest strategy to tackle the effect of tunneling would consist in performing full quantum calculations of the plasmonic response, as recently reported, within an atomistic *ab initio* or free electron description of the metal nanoparticles [9, 43–48, 50, 64]. However, because of numerical constraints, quantum calculations can only address systems which are much smaller than those of practical interest in plasmonics. A possible solution to this constraint consists in using model local dielectric functions that account for the quantum tunneling, in a way similar to the derivation of the macroscopic permittivity of a system from the microscopic quantum polarizabilities of the constituent atoms or molecules [65]. This can be achieved with the Quantum Corrected Model (QCM) [45, 66] that treats the junction between the nanoparticles as an effective medium mimicking quantum tunneling within the classical local dielectric theory. So far, the QCM has been shown to correctly reproduce the full quantum results in plasmonic dimer structures with a localized contact region supporting the tunneling current [9, 40–42, 48, 49]. In this work we study a very different system formed by a cylindrical metallic core and a cylindrical metallic shell, thus separated by a much more extended tunneling contact region between the core and shell metal surfaces, so-called cylindrical nanomatryushka (NM).

We first perform the quantum mechanical time dependent density functional theory (TDDFT) calculations of the optical absorption cross section of the cylindrical nanomatryushka. Owing to the large tunability of their plasmonic response and to the possibility of fabrication of these structures in small size with very narrow gaps between the core and the shell [12, 13], NM-like

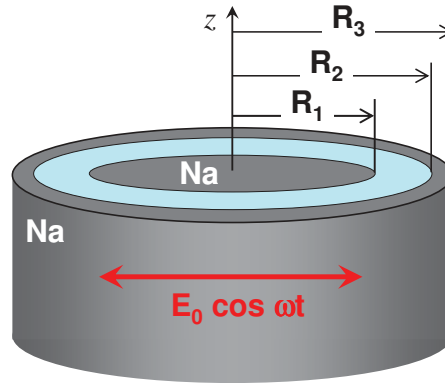


Fig. 1. Sketch of the geometry of the cylindrical nanomatryushka. The coaxial cylindrical core and cylindrical shell are infinite along the z -axis. The core has the radius R_1 ; the internal radius of the shell is R_2 , and the external radius of the shell is R_3 . The core and the shell are separated by the vacuum gap. The incident field with amplitude E_0 , and angular frequency ω is polarized perpendicular to the axis of the NM.

nanostuctures are of considerable practical and fundamental interest. The optical properties of NMs have been addressed within the classical electromagnetic theory framework in a number of publications [67–75]. It is only recently that the full quantum results have been reported for the spherical NM [76] showing the importance of tunneling between the core and the shell. The aim of the present study is twofold: (i) to follow the detailed evolution of the plasmonic resonances of the cylindrical NM upon variation of the size of the gap between the core and the shell, and (ii) to use the full quantum study as a benchmark for the QCM calculations. We focus on the quantum effects in this system because the standard classical calculation fails to describe the plasmonic response of the cylindrical NM for core-shell separations below 0.5 nm, while the QCM can reproduce well the quantum results. In addition to the previous studies of plasmonic dimer structures showing with tunneling regions localized around the contact point, our results for NMs extend the validity of the QCM to other geometries with more extended tunneling regions. Indeed, in the present case the tunneling current flows transversally through the entire core-shell gap. Along this lines, we also demonstrate that the QCM reproduces the quantum results obtained previously for the spherical NM [76], thus offering an efficient way to address tunneling effects in core-shell nanoparticles.

2. Model and computational aspects

The sketch of the cylindrical nanomatryushka in vacuum considered in this work is shown in Fig. 1. The infinite metallic cylindrical core and the metallic cylindrical shell are coaxial with the geometry set by the radius of the core R_1 , the internal radius of the shell R_2 , and the external radius of the shell is R_3 . Following the widely used notation, we will adopt the set (R_1, R_2, R_3) to characterize the NM structure [76]. The incident light is polarized perpendicular to the symmetry axis. To focus the discussion on the main subject of our interest – the role of the tunneling effect in the plasmonic response – and to facilitate the comparison with earlier published work on spherical nanomatryushkas, the region between the core and the shell is chosen to be vacuum. The results below are obtained for a fixed $R_2 = 90 a_0$ (48 Å), and $R_3 = 115 a_0$ (61 Å), while the radius of the core R_1 is varied. Here a_0 (0.53 Å) stands for the Bohr radius. The range of values considered for R_1 corresponds to the progressive reduction of the

width of the vacuum gap between the core and the shell, $S = R_2 - R_1$, from 20 Å down to the touching geometry ($S = 0$). This allows an analysis of the progressive emergence of the tunneling across the gap, and of its role in the evolution of the NM plasmonic modes into those of the uniform cylindrical nanowire.

In our quantum calculations the metallic core and the shell are described within the cylindrical jellium model (JM) as detailed previously [48, 49]. The valence electrons are bound by the uniform positive background charge representing the ionic cores. This background charge density is given by $n_0 = (4\pi r_s^3/3)^{-1}$, where r_s is the Wigner-Seitz radius. R_1 defines the position of the boundary of the positive background charge, the jellium edge, of the core. R_2 and R_3 define the inner and the outer jellium edges of the shell, respectively. Despite its simplicity, the JM correctly captures the collective plasmonic behavior of the conduction electrons, and it has demonstrated a good predictive power in the description of quantum effects in nanoparticle dimers, as follows from the comparison with experiments [9, 10] and with advanced full atomistic ab initio calculations [64]. We use the Wigner-Seitz radius r_s equal to 4 a_0 (2.12 Å) corresponding to Na metal. In this case the JM performs particularly well in the description of the interaction of the optical pulse with nanosized objects [77–80]. For noble metals, such as silver and gold, the contribution of the localized d-electrons to the screening [81, 82] imposes the introduction of a polarizable background [43] which would complicate the interpretation of the results, and obscure the comparison with the classical Drude and QCM model calculations. We emphasize that the qualitative conclusions drawn in this work are robust and independent of the particular choice of the density parameter.

The quantum calculations of the absorption cross-section are based on the the Kohn-Sham (KS) scheme of the density functional theory (DFT) [83]. We use the adiabatic local density approximation with the exchange-correlation functional of Gunnarsson and Lundqvist [84]. A detailed description of the numerical technique can be found in [44] by Marinica *et al.*, and in [49] by Teperik *et al.* First, the ground state electron density and Kohn-Sham orbitals are obtained in standard static DFT calculations. Using the axial symmetry allows to address the system with up to 290 electrons per 1 Å length. The structures are characterized by an overall work function of 2.9 eV, where the exact value depends on the core radius R_1 . At a second stage, the frequency ω -dependent absorption cross-section per unit length, $\sigma(\omega)$, is calculated from the electron density dynamics induced by an impulsive perturbation, within the time-domain time dependent density functional theory (TDDFT) approach.

$$\sigma(\omega) = \frac{4\pi\omega}{c} \text{Im}\{\alpha(\omega)\}. \quad (1)$$

In Eq. (1), $\alpha(\omega)$ is the dipolar polarizability (per unit length) of the system, and c is the speed of light in vacuum. Because of the small transverse size of the system, retardation effects are neglected for the present choice of the polarization of the incident electromagnetic wave.

Consistent with TDDFT, the classical electromagnetic calculations of the absorption cross-section have been performed within the quasistatic approximation [74] (see also [75] by H. Xu) using the local classical and the QCM approaches. Within the local classical approach the dielectric constant of the metal is described with the Drude model:

$$\epsilon(\omega) = 1 - \frac{\omega_p^2}{\omega(\omega + i\gamma)}, \quad (2)$$

where ω_p is the bulk plasma frequency of the metal and γ accounts for the damping. We use $\omega_p = 5.68$ eV and $\gamma = 0.218$ eV as obtained from the fit of classical results to TDDFT calculations for the isolated cylindrical nanowire of radius $R = 115 a_0$ (61 Å). These dimensions correspond to the geometry of the system with a fully closed gap between the core and the

shell. Note that the value of $\omega_p = 5.68$ eV is lower than the nominal plasma frequency for the bulk Na given by $\omega_b = \sqrt{4\pi n_0/m_e} = 5.89$ eV, with m_e the electron mass, and reflects the red shift of the dipolar plasmon from the classical $\omega_b/\sqrt{2}$ prediction. This red shift is the finite size effect resulting from the spill out of the electron density outside the metal boundaries, as has been thoroughly studied in the context of surface physics [77, 82, 85–89].

The QCM model [45, 66] describes the electron tunneling between the core and the shell by filling the core-shell gap with an effective dielectric medium described by a Drude model that depends on the gap separation distance S , similar to that in Eq. (2), as:

$$\epsilon_{\text{eff}}(S, \omega) = 1 - \frac{\omega_p^2}{\omega(\omega + i\gamma_{\text{eff}}(S))}. \quad (3)$$

The effective damping γ_{eff} models the transition from a resistive to a conductive nature of the junction as a function of the gap separation S . Consistently with the dependence of the electron tunneling probability on the size of the gap, γ_{eff} is given by

$$\gamma_{\text{eff}} = \gamma_0 e^{[S/\Delta]}. \quad (4)$$

For the tunneling contact between Na metal surfaces we use $\epsilon_\infty = 1$ in Eq. (3), and in Eq. (4) we use $\gamma_0 = 0.218$ eV and $\Delta = 0.75$ Å [45, 66]. For sufficiently large separation distances, $S \rightarrow \infty$, the effective damping $\gamma_{\text{eff}} \rightarrow \infty$, and the QCM becomes exactly equivalent to the local classical approach. In this situation, no tunneling is possible and the vacuum gap limit is retrieved with $\epsilon_{\text{eff}}(S, \omega) = 1$. For $S \rightarrow 0$, the junction becomes metallic with permittivity equivalent to that of the bulk metal so that the NM responds as an homogeneous metallic cylinder.

3. Results and discussion

3.1. Plasmon modes of a cylindrical nanomatryushka

We first characterize the linear optical response of the cylindrical NM with particular emphasis on the assignment of the plasmonic modes. To this end we base our discussion on the classical quasistatic results which provide a good reference for the full quantum calculations of the NM with large gap, and thus no tunneling. The classical results have also the advantage of featuring well defined many-body plasmonic modes, not affected by the interaction with single-particle electron-hole pair excitations which are typical for the quantum TDDFT calculations in systems of small size like this [47, 79, 80]. In Fig. 2(a) we show the absorption cross section per unit length of an individual cylindrical nanowire with external radius $R = 61$ Å (black dashed line). This would correspond to the limiting case of a NM with zero width gap $S = 0$. Our calculations also show the results for a cylindrical shell with internal radius $R_2 = 47.7$ Å, and external radius $R_3 = 61$ Å, (blue line), and finally, the case of a cylindrical NM with the same shell as in the previous case, and a core of radius $R_1 = 37$ Å, i.e. a cylindrical (37, 47.7, 61) Å NM (red line). The dimensions of the system in units of the Bohr radius are (70, 90, 115) a_0 . In practice, atomic units are the natural choice for quantum studies, and while in most of the cases we give dimensions in Å for convenience of the broad audience, our TDDFT calculations use atomic units. For the individual nanowire, the TDDFT data is also presented (green line) along with the classical results to validate the quality of the classical Drude modeling of the optical response in this case.

The absorption cross section of the individual cylindrical nanowire representative for the core of the nanomatryushka is dominated by the single plasmon resonance at surface plasmon frequency $\omega_- = \omega_p/\sqrt{2}$, where ω_p is the bulk plasma frequency in the Drude model of the dielectric function given by Eq. (2). As already pointed out, because of the nonlocal screening and the small radius of the nanowire, in our calculations $\omega_- = 4.02$ eV is red shifted with

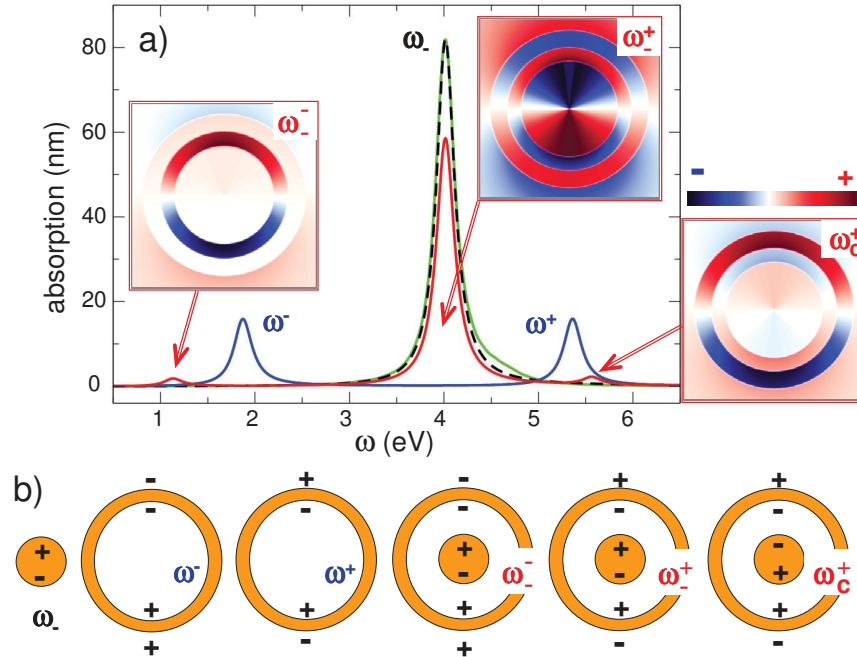


Fig. 2. (a) Absorption cross section per unit length. The green line shows the TDDFT result for an individual nanowire with radius $R = 61 \text{ \AA}$. The rest of the results are obtained using classical electromagnetic theory within a nonretarded approximation. Black dashed line: individual nanowire with radius $R = 61 \text{ \AA}$. Blue line: cylindrical shell with internal radius $R_2 = 47.7 \text{ \AA}$, and external radius $R_3 = 61 \text{ \AA}$. Red line: cylindrical $(37.1, 47.7, 61) \text{ \AA}$ nanomatryushka. The inserts show the direction of the radial electric fields associated to the ω_- , ω_+ , and ω_c^+ modes of the core-shell structure. The arrows indicate the corresponding absorption resonances. (b) Schematic charge distribution for the different plasmonic modes identified in a).

respect to the corresponding surface plasmon frequency of the Na metal, 4.16 eV [47, 77, 82, 85–89]. The distribution of the plasmon-induced charges of this mode is schematically shown in Fig. 2(b). The optical absorption of the cylindrical shell is characterized by a low frequency bonding resonance ω^- , and a high frequency antibonding resonance ω^+ [79, 80] with plasmon charges separated, respectively, over the entire shell or across each shell boundary, as shown in Fig. 2(b). In the NM, the ω_- dipole mode of the core nanowire hybridizes with the ω^- and ω^+ dipole modes of the nanoshell giving rise to the ω_- , ω_+ , and ω_c^+ resonances. The lowest energy bonding hybridized resonance ω_- at 1.1 eV is formed by the bonding shell mode ω^- with an admixture of the core ω_- resonance. The most prominent ω_+ absorption resonance of the nanomatryushka at 4 eV is formed primarily by the symmetric coupling of the ω_- core mode with the ω^+ shell resonance. Finally, the antisymmetric coupling of the ω_- core mode with the ω^+ shell resonance forms the anti-bonding resonance of the NM, ω_c^+ (here we use the terminology from [76] by Kulkarni *et al.*). As follows from Fig. 2(b), the charge distribution of the ω_+ mode corresponds to the parallel core and shell dipoles so that this mode strongly interacts with the incident electromagnetic wave. The ω_- and ω_c^+ modes are characterized by antiparallel core and shell dipoles, therefore the corresponding absorption resonances are weak in this case.

The near-field distribution of the plasmon resonances is shown in the inserts of Fig. 2(a).

Owing to the opposite sign of the plasmon induced charges at the surface of the core and inner surfaces of the shell, the lowest energy bonding hybridized mode ω_- is characterized by a strong field enhancement inside the core-shell gap. On the other hand, because the core and shell dipoles are antiparallel, the fields are weak outside the structure. Similar to ω_- , and because of the induced charge configuration, for the ω_+ resonance the fields in the gap are also strongly enhanced. For this mode the core and shell dipoles are aligned. This leads to strong induced fields outside the structure consistent with the most intense peak in the absorption cross section at ω_+ . The core character of the ω_+ resonance clearly appears in the structure of the corresponding induced fields showing a bright core region. The ω_c^+ mode is characterized by the opposite sign of the core and shell dipoles and by the same sign of plasmon-induced charges across the gap. The fields are thus low in the gap, core and vacuum regions. Strong plasmon-induced fields are only calculated inside the shell consistent with the shell character of this plasmon mode. It should be noted that the character of the modes and their near field distribution is analogous to that of a spherical NM [68–73, 76]. The resonance energies are however different because of the different dimensionality of the problem. Indeed, for a Drude metal, the quasistatic cylindrical core plasmon is at $\omega_- = \omega_p/\sqrt{2}$, while the spherical core plasmon is at $\omega_- = \omega_p/\sqrt{3}$.

From a qualitative analysis of the induced charge distributions and near fields of the modes, it is possible to presume that quantum effects might be relevant when the gap separation between the core and the shell in the NM decreases. This situation can occur by means of an increase of the core radius R_1 . Analogous to the spherical NM case [76], because of electron tunneling between the core and the shell, the gap becomes conductive for small S (narrow gaps). In the touching limit ($S \rightarrow 0$), a situation analogue to that of the continuous metallic cylinder can be reached even prior to the direct geometrical contact at $R_1 = R_2$. In such a situation, the modes ω_- and ω_c^+ would disappear and the mode ω_+ would evolve into that of the metallic cylinder with a radius given by the external radius of the shell $R_3 = 61 \text{ \AA}$. Since the ω_- and ω_+ resonances are characterized by a distribution of opposite charges across the gap, the effect of tunneling in these modes can be expected to be stronger than for the ω_c^+ resonance. The above discussion is fully confirmed by the quantum TDDFT results presented in the next section.

3.2. Role of quantum tunneling across the gap

In the left columns of Fig. 3 we show the waterfall plots of the absorption cross section of a NM per unit length. The results are shown as a function of the frequency ω of the incident radiation polarized perpendicular to the symmetry axis of the system. The calculations were performed over a wide frequency range, and for various gap sizes, from well separated core and shell, down to the situation of conductive contact at $S = 0$. Different panels of the figure correspond to the results obtained within classical calculations using the Drude model of the metal permittivity (top), within the full quantum TDDFT (center), and with the quantum corrected model (QCM) (bottom). The system geometry is defined by $(R_1, 47.7, 61) \text{ \AA}$, where the core radius has been varied within the limits $26.5 \text{ \AA} \leq R_1 \leq 47.7 \text{ \AA}$ consequently, allowing to vary the size of the vacuum gap according to $S = 47.7 \text{ \AA} - R_1$. The gross features of the results are similar for the classical, quantum and QCM descriptions of the system. These results resemble those reported in the literature for similar core-shell systems [67–73, 76]. With an increasing value of the core radius, R_1 (smaller S), the interaction between the induced charges across the gap increases, and the pair of hybridized plasmons with shell character display a red-shift (ω_-), and a blue-shift (ω_c^+), respectively. Because of the mutual compensation between the core and the shell dipoles for these modes [see Fig. 2(c)], their spectral features progressively loose their intensity in the absorption spectrum. For $R_1 \rightarrow R_2$, the ω_- and ω_c^+ resonances can be hardly distinguished in the spectrum. The differences between the quantum and the classical calculations, particularly

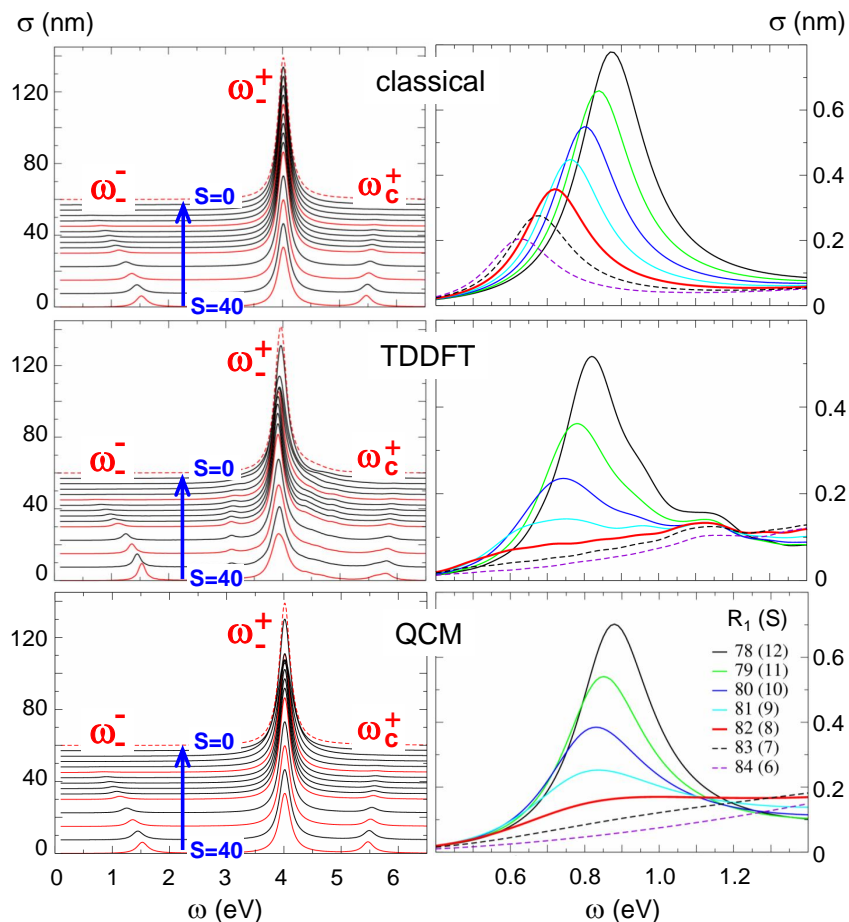


Fig. 3. Waterfall plot of the absorption cross section per unit length, σ , of a cylindrical nanomatryushka defined by $(R_1, 47.7, 61)$ Å, or equivalently $(R_1, 90, 115)$ a_0 , where the Bohr radius $a_0 = 0.53$ Å, calculated using classical electromagnetic theory (top), TDDFT (center) and the Quantum Corrected Model (QCM) (bottom). Results are given as a function of the frequency ω of the incident radiation for different core radii R_1 . The left panels show the results within a large ω range showing all the resonances described in Fig. 2. R_1 varies within the limits $50 a_0 \leq R_1 \leq 90 a_0$ ($26.5 \text{ \AA} \leq R_1 \leq 47.7 \text{ \AA}$), corresponding to gap separation distances, S , from $40 a_0$ down to 0, as indicated by the blue arrows on the spectra. For clarity, a vertical shift is introduced to each absorption spectrum. The curves are displayed in red every $10 a_0 \approx 5.3 \text{ \AA}$ of R_1 -change. The lowest absorption spectrum in each panel corresponds to $R_1 = 50 a_0$ ($S = 40 a_0$), and the red dashed curve on top ($S = 0$) is used as a reference for the absorption spectrum of the solid metallic cylinder with external radius $R = 115 a_0$ (61 \AA). The plasmonic modes responsible for the peaks in the absorption cross-section are labeled in each panel. ω_-^+ stands for the bonding hybridized resonance, ω_0^+ for the hybridized resonance with a dominantly core character, and ω_c^+ for the anti-bonding resonance of the nanomatryushka. The right panels focus on results for core radii R_1 in the range of $78 a_0 \leq R_1 \leq 84 a_0$ ($41.3 \text{ \AA} \leq R_1 \leq 44.5 \text{ \AA}$) at the frequency range of the ω_-^+ plasmon of $0.4 \text{ eV} \leq \omega \leq 1.4 \text{ eV}$. These are the conditions where the effect of the resonant electron transfer on the bonding hybridized plasmon ω_-^+ is most prominent. The correspondence between the color used for the absorption spectra and the value of the core radius R_1 is given at the lower right panel of the figure. R_1 is indicated in units of a_0 and the number in parenthesis gives the corresponding size of the gap, S , between the core surface and the inner surface of the outer shell.

for the ω^- mode, cannot be observed in the left-hand side spectra of Fig. 3, since their scale is set by the main peak in the absorption cross section (the core resonance ω^+). For a vanishing gap, this prominent resonance evolves into the dipolar resonance of the full metallic cylinder with radius $R_3 = 61 \text{ \AA}$. It is worth mentioning that for a small R_1 (large S), the results within the TDDFT for the core ω^+ plasmon show a red shift because of the electron spill-out effect and the nonlocal screening, [77, 82, 85–89] as well as additional broadening because of the increased Landau damping. It is also possible to notice some additional structures in the TDDFT absorption cross-section due to the presence of electron-hole pair excitations [47, 79, 80]. The left-lower panel of Fig. 3 shows that the QCM reproduces well the details of the spectra. For example, it captures the abrupt change of the main absorption peak at small gap separation distances (spectra on the top), similarly to that present in the TDDFT calculations, whereas the classical calculations show a smoother evolution. This abrupt change at $S \approx 1 \text{ \AA}$ is linked with the lowering of the potential barrier separating the core and the shell below the Fermi level. Under these conditions, the electrons flow through the gap quasi-freely forming a continuous metallic connection.

As we discussed in the previous section, the effect of electron tunneling is expected to be the strongest for the ω^- resonance, since it is characterized by induced plasmon charges of opposite sign across the gap, capable of supporting a strong tunneling current. To reveal the role of quantum tunneling in the NM gap, in the right panels of Fig. 3 we zoom into the spectral range of frequencies of the ω^- resonance, showing the evolution of this lowest energy mode as the gap becomes smaller. We compare results within the Classical Drude (top), TDDFT (center) and QCM (bottom) for values of core radius R_1 in the range of $78 a_0 \leq R_1 \leq 84 a_0$ ($41.3 \text{ \AA} \leq R_1 \leq 44.5 \text{ \AA}$), corresponding to gap sizes in the range of $6 a_0 \leq S \leq 12 a_0$ ($3.2 \text{ \AA} \leq S \leq 6.4 \text{ \AA}$). As found in previous calculations of the plasmonic dimer structures [43–45, 47, 48, 64], tunneling effects progressively appear for narrow gaps. In the classical calculations, the ω^- resonance is always present albeit being attenuated and red-shifted with increasing R_1 (decreasing gap distance S). The quantum TDDFT results show a distinct qualitative behavior. For the smallest value of the core radius considered (large S) in Fig. 3, $R_1 = 78 a_0$, the ω^- resonance is in agreement with the classical prediction. However, the resonance is fully quenched for $R_1 = 82 a_0$. For this very narrow gap of $S = 8 a_0$, electron tunneling across the gap neutralizes the induced plasmonic charges of opposite sign at the facing surfaces of the core and the shell, leading to the disappearance of this bonding hybridized plasmon. This is in contrast to the classical calculations where this gap mode is always present for any $S \neq 0$. In the lower panels of Fig. 3, we can observe that the TDDFT results are well reproduced by the QCM calculations, including the progressive broadening and final quenching of the ω^- resonance for narrowing gaps due to the increasing resistive tunneling losses. The full quenching of the gap plasmon due to tunneling is not considered in the classical calculations (top right panel), but it is captured by the QCM. This effect can be clearly appreciated, for instance by comparing the spectra in red lines on the three right hand side panels of Fig. 3. Finally, the high energy antibonding mode ω_c^+ is not so affected by quantum tunneling due to the symmetric distribution of charges at both sides of the gap [see Fig. 2(c)]. Classical and TDDFT calculations give practically the same results in this case for all separation distances (including the narrowest ones), therefore the QCM does not bring any essential improvement for this mode.

In Fig. 4 we show the enhancement \mathcal{F} of the field in the middle of the gap, as obtained with the classical Drude, QCM and full quantum TDDFT approaches. The enhancement is defined as the ratio of the total E_t and incident E_{in} fields, $\mathcal{F} = |E_t/E_{in}|$, measured at position $R = (R_1 + R_2)/2$ along the axis defined by the electric field polarization vector of the incident plane wave. The field enhancement has been calculated for the incident electromagnetic wave, resonant with the energy of the hybridized ω^- mode and with the ω^+ mode. For a size of the

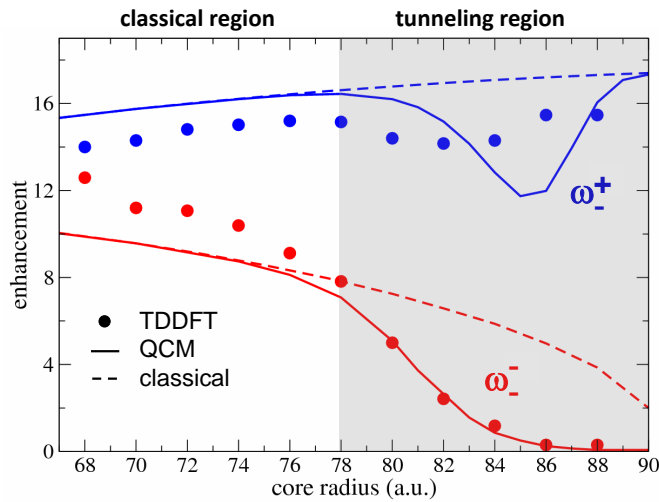


Fig. 4. Resonant field enhancement \mathcal{F} in the middle of the gap between the core and the shell of a NM, defined as the ratio of the total E_t and the incident E_{in} fields, $\mathcal{F} = |E_t/E_{in}|$, measured in the middle of the gap at $R = (R_1 + R_2)/2$ in the axis defined by the polarization of the incident field. Dots represent the TDDFT results, dashed lines represent results obtained using classical Drude calculations, and solid lines represent the QCM results. Red color is used for the data at the frequency of the lowest energy bonding hybridized resonance ω_-^- , and blue color for the data at the frequency of the main absorption peak labeled as the ω_+^+ resonance. The shaded background separates the region where tunneling occurs from the classical region.

gap, S , below 6 \AA (core radius above $78 a_0$) the quantum TDDFT results show distinct differences with respect to the classical predictions (area marked with a shaded background in Fig. 4). The onset of the electron tunneling between the core and the shell comes along with the disappearance of the ω_-^- resonance, and thus with a pronounced decrease of the field enhancement. Eventually \mathcal{F} is zero for small gap sizes where the limit of the homogeneous metallic cylinder is reached prior to direct physical contact between the core and the shell at $R_1 = R_2$. The QCM correctly reproduces the results of the quantum TDDFT, including a decrease of the field enhancement at the ω_+^+ resonance for intermediate tunneling distances. Indeed, the resistive tunneling losses lead to a certain broadening of the plasmon peak which results in a moderate decrease of the corresponding field enhancement. For vanishing separation, $S \rightarrow 0$, the junction becomes conductive and \mathcal{F} tends to the characteristic value of a homogeneous metallic cylinder of radius R_3 .

The ability of QCM to describe the quantum results has been reported in previous calculations for spherical and cylindrical dimer structures with gaps characterized by narrow contact regions which allow for the presence of tunneling current. In these systems the progressive disappearance of the bonding dipole plasmon mode and the appearance of the charge transfer plasmon mode prior to direct contact between the nanoparticles has been addressed within the quantum TDDFT calculations. These features are correctly reproduced with the QCM, while classical theories fail to address the spectral behavior, even qualitatively. Already at finite junction sizes the particles forming the dimer are conductively connected showing the characteristic charge transfer plasmon modes [22, 52–54, 56, 57]. In the present work we observe the same physics, with the core and the shell of the nanomatryushka being conductively connected prior

to the direct contact between their surfaces, and thus effectively forming the uniform metallic cylinder. However, differently to plasmonic dimer structures, the tunneling current in the case of a cylindrical NM flows over the whole extended gap region, a substantial dimensional difference that makes the NM an appropriate system to test quantum effects in plasmonics.

3.3. Spherical gold nanomatrixushka

The quantum effects described here for the cylindrical core-shell NM structure are similar to those found in the TDDFT study of the spherical gold NM [76]. Therefore, we also analyze now the performance of the QCM model in the spherical case. We use the QCM to calculate the absorption cross section of a gold NM within the non-retarded quasistatic approximation. This choice is justified considering the size of the studied system (external radius below 8 nm),

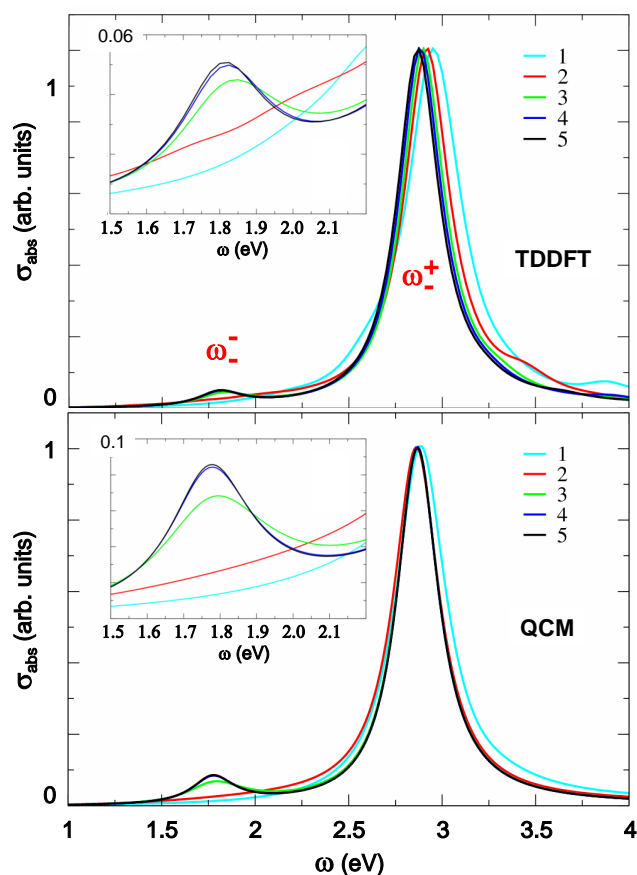


Fig. 5. Absorption cross section, σ_{abs} , for a spherical gold nanomatrixushka as a function of frequency ω . The results are normalized to the absorption maximum. Different NMs are considered whose dimensions are defined by $\lambda \times (R_1 = 8.5, R_2 = 9.5, R_3 = 15.9) \text{ \AA}$ where the values of λ ranges from 1 to 5, as displayed in the inset. R_1 is the core radius. R_2 , and R_3 stand respectively for the internal and external radius of the shell. Upper panel: quantum results from TDDFT calculations from [76] by Kulkarni *et al.* Lower panel: current results based on the QCM. The bonding hybridized resonance ω_- , and the main absorption peak of the core resonance ω_+ are indicated in the upper panel. The graphs in the insets show the respective zooms into the low-energy bonding hybridized resonance.

and it is consistent with non-retarded calculation of the potentials within TDDFT [76]. For the sake of comparison, we use the Drude-like model for the dielectric permittivity of the classical metal as proposed by Kulkarni *et al.* [76], based on the jellium model of gold used in their quantum calculations of the optical absorption:

$$\varepsilon(\omega) = \varepsilon_{\infty} - \frac{\omega_p^2}{\omega(\omega + i\gamma)}, \quad (5)$$

with $\varepsilon_{\infty} = 8$, $\omega_p = 9.07$ eV, and $\gamma = 0.27$ eV.

Within the QCM model, the effective dielectric medium in the gap, ε_{eff} , is defined by the frequency, and separation dependent dielectric constant,

$$\varepsilon_{\text{eff}}(S, \omega) = \varepsilon_{\infty} - \frac{\omega_p^2}{\omega(\omega + i\gamma_{\text{eff}}(S))}, \quad (6)$$

where $\gamma_{\text{eff}}(S)$ is given by Eq. (4) with $\Delta = 0.4$ Å [45, 66].

Figure 5 presents the frequency dependent optical absorption cross section, $\sigma_{\text{abs}}(\omega)$, for five spherical NM geometries defined by the scaling of a basic (8.5, 9.5, 15.9) Å NM structure, following the form $\lambda \times (8.5, 9.5, 15.9)$ Å, with $\lambda = 1, 2, 3, 4, 5$. This scaling [76] is implemented to rely on the invariance of the optical properties that classical electromagnetic calculations performed within a non-retarded approximation yield. The absorption cross section should be identical for scalable systems with scale factor λ^3 . Thus, any departure from the universal behavior can be associated with a signature of a quantum effect. The upper panel of Fig. 5 reproduces the quantum results of Kulkarni *et al.* [76], and the lower panel of Fig. 5 shows the absorption spectra obtained within our QCM calculation. For large gap sizes (4 Å and 5 Å), tunneling across the gap is not efficient and the results show the universal behavior pointed out above. When the gap size is reduced to 3 Å, the electron tunneling through the gap increases enough to lead to a visible attenuation of the ω_{-} resonance. Finally, similar to the cylindrical NM case, when the gap size is reduced below 2 Å ($4 a_0$), the tunneling current across the gap becomes large so that the lowest energy bonding hybridized resonance is quenched. This change of the absorption spectra exceeds the capabilities of the classical theory to treat such extreme gaps, as pointed out in [76] by Kulkarni *et al.* However the TDDFT results are well reproduced with the QCM, fully confirming the good performance of the latter to also address the optical properties of a spherical geometry with an extended tunneling contact.

4. Summary and conclusions

In conclusion, we tested the applicability of the quantum corrected model in systems which show an extended tunneling contact region between metallic surfaces. To this end we compared the results of the optical response calculated with the QCM and with full quantum Time Dependent Density Functional Theory for the case of a cylindrical nanomatryushka: the cylindrical core-shell structure, where the metallic core and metallic shell are separated by a vacuum gap. We considered a metallic system made of Na because the free-electron character of the Na valence electrons allows for a jellium model description. Reasonably large-size system with well developed plasmonic modes can be addressed in this way at the fully quantum level. Moreover, in this case the material permittivity can be well described with the Drude model which eases the comparison between quantum, classical electromagnetic, and QCM results.

We obtained that when the core-shell gap is reduced below 5 Å, the optical response is determined by the quantum tunneling of conduction electrons across the potential barrier separating the core and the shell. Our results agree with earlier calculations on plasmonic dimer structures. Specifically, a decreasing junction separation leads to the disappearance of the lowest

energy bonding hybridized plasmon mode and a quenching of the field enhancement at the corresponding frequency. The limit of the continuous and homogeneous cylinder is reached prior to the direct contact between the core and the shell. The classical local Drude description fails to reproduce the observed effects since it does not account for tunneling. In contrast, the QCM results are found to be in good agreement with the full quantum calculations.

For large gap sizes, electron tunneling is negligible and there is an overall agreement between TDDFT, classical Drude, and QCM calculations. Therefore, as a whole, the QCM performs very well over the entire range of core-shell gap sizes S studied here. We note however that the TDDFT results show some features that are not reproduced with classical models: the size-dependent frequency shifts of the plasmonic modes due to the nonlocal screening, the size-dependent broadening because of the Landau damping and, finally, additional spectral features because of electron-hole pair excitations.

We have also performed the QCM calculations of the spherical gold NM, where previous results of quantum calculations were available [76]. The spectral trends are similar to those found for the cylindrical sodium NM. The QCM and the quantum absorption spectra are in very good agreement which fully validate the applicability of the QCM to general systems characterized by extended tunneling contact regions between metallic surfaces. Together with the earlier studies in plasmonic dimers that showed narrow tunneling contacts, our results extend the range of applicability of the QCM. Elucidating the main physics in tunneling plasmonic gaps shows enormous potential with important consequences in the accurate description of far- and near-fields in extreme morphologies, as well as in the control of non-linear effects associated to ultranarrow gaps such as in rectification.

Acknowledgments

We gratefully acknowledge V. Kulkarni, E. Prodan, and P. Nordlander for providing results of the TDDFT calculations of the absorption spectra of the spherical NM, and Rubén Esteban for fruitful input on the Quantum Corrected Model. M.Z. acknowledges financial support from the Departamento Administrativo de Ciencia, Tecnología e Innovación-COLCIENCIAS and Facultad de Ciencias from Universidad de los Andes. J.A. acknowledges financial support from Project "Plasmogap" (FIS2013-41184-P) of the Spanish Ministry of Economy and Competitiveness (MINECO), project Eortek Nanogune'14 of the Department of Industry of the Basque Government, and project IT756-13 of consolidated groups from the Department of Education of the Basque Government.